FDTD Verification of Deep-Set Brain Tumor Hyperthermia Using a Spherical Microwave Source Distribution

David Dunn, Carey M. Rappaport, and Andrew J. Terzuoli, Jr.

Abstract—**Although use of noninvasive microwave hyperthermia to treat cancer is problematic in many human body structures, careful selection of the source electric field distribution around the entire surface of the head can generate a tightly focused global power density maximum at the deepest point within the brain. An analytic prediction of the optimum volume field distribution in a layered concentric head model based on summing spherical harmonic modes is derived and presented. This ideal distribution is then verified using a three-dimensional finite difference time domain (FDTD) simulation with a discretized, MRI-based head model excited by the spherical source. The numerical computation gives a very similar dissipated power pattern as the analytic prediction. This study demonstrates that microwave hyperthermia can theoretically be a feasible cancer treatment modality for tumors in the head, providing a well-resolved "hot-spot" at depth without overheating any other healthy tissue.**

I. Introduction and Background

CANCER HAS been a leading cause of death for several decades, hence research in new modalities to treat the disease is of great interest. Along with great advances in chemotherapy and ionizing radiation, hyperthermia treatment has been successfully used to destroy cancer cells.

Noninvasive microwave hyperthermia has not lived up to the potential originally envisioned for it, because of the difficulty in focusing electromagnetic power at depth in high water content (HWC) biological tissue. HWC tissue, which includes muscle, blood, and organ tissue, has relatively high dielectric constant and conductivity. It absorbs power quickly while rapidly attenuating waves propagating through it, preventing deep wave penetration. Unfortunately, most cancerous tumors occur in HWC tissue, so unless one makes clever use of constructive interference, it is difficult to heat only the tumor.

Focusing an external microwave surface source increases the power deposited at a deep target, but unless the target power density level is greater than the power density at the tissue surface or at any other position in the tissue volume, healthy tissue will be harmed. Even though focusing yields much greater target heating, focusing alone may still be impractical because of excessive heating of healthy intervening tissue. The only hope for safe and effective heating of a tissue volume occurs when the source surrounds the volume. Even then, appropriate frequencies and source distributions must be utilized. In this study, previous promising analytic work on an idealized spherical volume is extended to more realistic models of the human head. First, a three-layer analytic head model using measured electrical parameters for brain gray matter, skull bone, and HWC bolus is considered, then the finite difference time domain (FDTD) method [1] is used to calculate the precise electric field distribution necessary for deep, focused heating.

The FDTD method and other computational methods have been used in the past in several studies to determine electromagnetic effects within biological tissue [2], with a particular interest in human head exposure to cellular telephone radiation [3]–[7]. However, FDTD has not been used in a deep hyperthermia treatment scenario, in which the verification of focused target heating with minimal overheating of healthy tissue is essential.

II. Analytic Formulation and Optimization

The original work using a spherical source distribution for symmetric [8] and eccentric [9] targets was based on a single uniform sphere of HWC tissue. Although the human head is not spherical, electric field sources can be placed on the surface of a spherical bolus filled with an HWC tissue-like fluid (such as sterile saline solution). This bolus serves both to help match the exterior field to the head, and to act as a skin surface cooler. This preliminary research demonstrated that a spherical source distribution could be optimized to effectively irradiate the center of a 9.45-cm-radius uniform sphere of HWC tissue. The model considered was for the worst case, assuming the greatest tissue loss characteristics—for each frequency—in the largest possible sphere for which a central global maximum could be found.

Although it may be that healthy tissue survives more heating than diseased tissue, or that thermal conduction and differential perfusion rates might improve the relative heating in tumor volumes, to ensure that *no* healthy tissue region is overheated, it is essential that the dissipated power density is everywhere below the level at the tumor target. It should be noted that specific absorption rate (SAR) is not as useful a measure of this overheating as power density (which has units of watts/m^3). Normalizing this power density across the head to the value at the focal target establishes a unitless measure of hyperthermia

Manuscript received October 26, 1995; revised March 20, 1996.

D. Dunn is with the 20th Intelligence Squadron, Offutt AFB, NE 68113 USA.

C. M. Rappaport is with the Center for Electromagnetics Research, Northeastern University, Boston, MA 02115 USA.

A. J. Terzuoli, Jr. is with the Graduate School of Engineering, Air Force Institute of Technology, Dayton, OH 45433 USA.

Publisher Item Identifier S 0018-9480(96)07020-2.

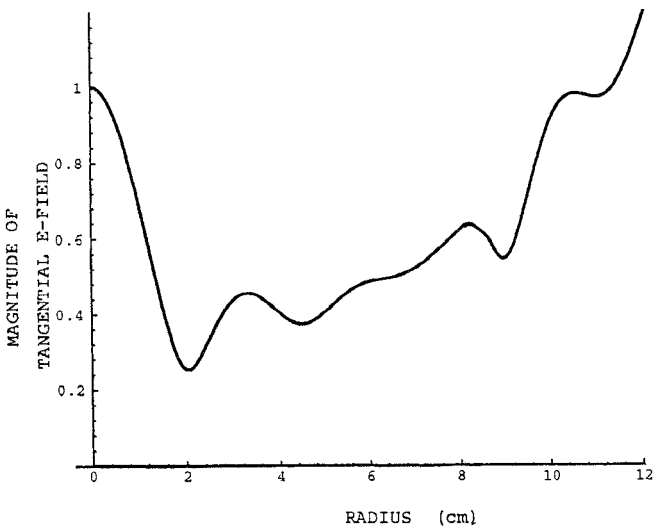

Fig. 1. Tangential electric field magnitude in a three-layer spherical shell idealized human head model, normalized to values at the center.

safety: for those areas where the normalized power density exceeds unity, overheating is likely.

The research with the uniform spherical model determined the optimal frequency f_o of those available in the Industrial, Scientific, and Medical (ISM) frequency bands to be 915 MHz. As the frequency increases above this value, focal resolution increases, but penetration depth is reduced; 915 MHz provides the best tradeoff between resolution and depth [8].

It should be emphasized that although multiple frequency illumination is possible and may be preferable for practical reasons, the essential determinating factor of focal resolution for deep target heating is the choice of the optimum continuous wave frequency. Since the field distributions for each frequency are orthogonal to one another, a multiple frequency excitation—such as a pulse in the time domain—will only penetrate and resolve as well as its best monochromatic component. Other frequency components may certainly increase power at the focus, but will also add power everywhere else: at the surface, at the minima in the optimum frequency pattern, and most importantly at the local pattern maxima.

An optimized volume field distribution can be found using solutions to the spherical vector wave equation. As demonstrated in [8], only the lowest-order mode gives nonzero contribution to power at a target at the origin in the center of a sphere. Therefore, adding higher-order harmonics does not affect the focal power density, but if carefully weighted, can reduce other local power maxima, specifically at the sphere surface. The odd harmonics—which are symmetric about the equator—are added out of phase with the first harmonic at the sphere surface, thereby decreasing the power density at the equator, increasing the power density near the poles, and keeping the same power density at the central focus.

For the three-layer analysis, the inner spherical volume is modeled as gray matter, while the skull is now slightly more realistically modeled as a concentric shell with inner and outer radii 8.2 and 8.7 cm—representing the average position of the real eccentric skull. An HWC tissue spherical bolus with electrical characteristics of skin tissue is specified as the final layer surrounding this bone shell. Certainly other bolus liquids could be used—such as lossless distilled water, which would not be directly heated by the microwave excitation—but avoiding a fourth spherical shell simplifies the model considerably without compromising the general field behavior within the head. As this analytic model is primarily intended to determine whether a global power maximum is possible, as well as the source distribution that generates this target maximum, practical considerations such as patient comfort and actual antenna design are neglected in this idealized analysis, but obviously need to be considered before a realistic application is developed.

The spherical harmonic solution to the vector wave equation with circumferential symmetry in each concentric medium layer m (where $m = 1$ is the innermost sphere) is given by [10]

$$\begin{aligned}\overline{E}^m(\overline{r}) = \sum_{n=1}^{\infty}\Bigg\{ & \hat{r}\frac{n(n+1)}{k^m r}(A_n^m j_n(k^m r) \\ & + B_n^m y_n(k^m r))P_n(\cos\theta) \\ & + \hat{\theta}\Big(A_n^m\Big[j_{n-1}(k^m r) - \frac{n}{k^m r}j_n(k^m r)\Big] \\ & + B_n^m\Big[y_{n-1}(k^m r) - \frac{n}{k^m r}y_n(k^m r)\Big]\Big) \\ & \cdot \frac{\partial}{\partial\theta}P_n(\cos\theta)\Bigg\} \end{aligned} \tag{1}$$

with

$$k^m = \frac{\omega}{c}\sqrt{\epsilon'^m - j\frac{\sigma^m}{\omega\epsilon_0}}$$

where $\omega = 2\pi f_0$, P_n, j_n, and y_n are the nth-order Legendre and nth-order spherical Bessel and Neumann functions, respectively; A_n^m and B_n^m are the nth complex weighting coefficients for the mth layer. Note that to keep field solutions nonsingular, $B_n^1 = 0$, and since for destructive symmetry only odd harmonics are used, implying all even n coefficients are zero.

For the original study with a single uniform sphere, $B_n^m = 0$, and only $A_n^1 \neq 0$. The coefficients for the optimization for 915 MHz at a radius of 9.45 cm are: $A_1^1 = 1.21 + 0.89j$, $A_3^1 = 0.19 - 0.055j$, and $A_5^1 = 0.01 - 0.019j$. For this choice of coefficients, the highest power density at the sphere surface is just equal to the power density at the center. Hence this surface electric field distribution is that required to safely heat the largest possible spherical HWC tissue volume.

In the three-layer analysis, the mathematics is considerably more challenging. The five coefficients for each polar mode, A_n^1, A_n^2, A_n^3, B_n^2, B_n^3 must be found by equating the tangential electric E_θ and magnetic H_ϕ fields at each of the two shell boundaries, $r = 8.2$ and $r = 8.7$ cm. The electromagnetic characteristics of the three tissue types—along with others not used until later—are given in Table I.

The tangential electric field magnitude $|E_\theta|$, normalized to its value at the origin and plotted as a function of radius from the center of the sphere in the equatorial plane ($z = 0$) for the first mode $n = 1$, is shown in Fig. 1. The material boundaries are identified by vertical lines. The dissipated power density in

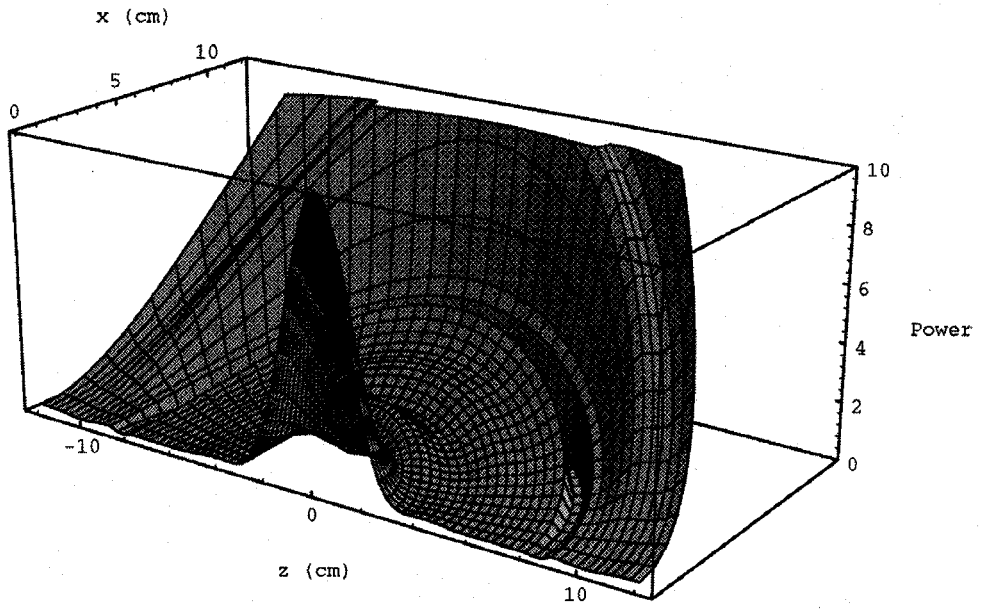

Fig. 2. Analytically computed dissipated power density in the cross section of the idealized three-layer head.

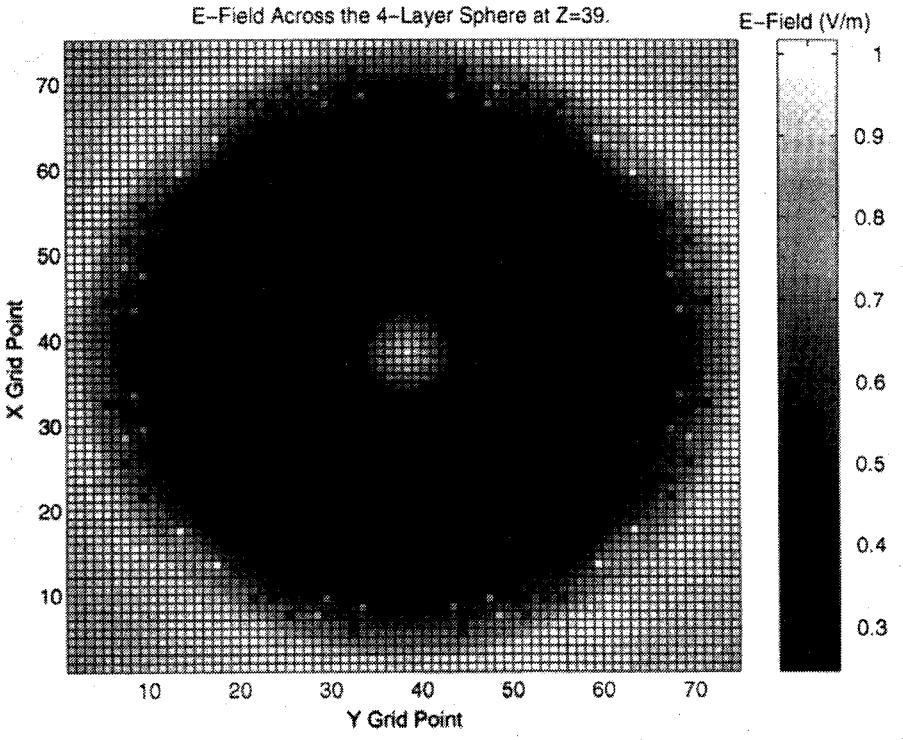

Fig. 3. The electric field distribution across an x-y cut of the four-layer sphere at $z = 39$.

each shell—given by $P^m = \sigma^m(|E_r^m|^2+|E_\theta^m|^2)/2$—is shown in Fig. 2 throughout half of the entire vertical cross section. Note that the dissipated power is almost entirely confined to the vicinity of the focal target at the origin, with almost no power dissipated in the rest of the healthy tissue inside the head. Also, the lower conductivity in the bone layer clearly generates a 0.5-cm-thick valley at the spherical shell starting at $r = 8.2$ cm. From Fig. 2, the $\sin^2\theta$ power density variation of the first mode is visible, rising from zero at the poles to its maximum values at the equator. In the bolus region, $r > 8.7$ cm, the power density rises rapidly with radius, but since this region is outside the head, none of this power heats any biological tissue. Since there is almost no power in the healthy tissue, other higher modes in (1) do not need to be included in the total electric field; the fundamental is sufficient for this choice of frequency.

III. Numerical Verification

The analytical optimization discussed above is verified using FDTD computation with laminated spheres in a manner discussed in [11]. Computations were performed using a

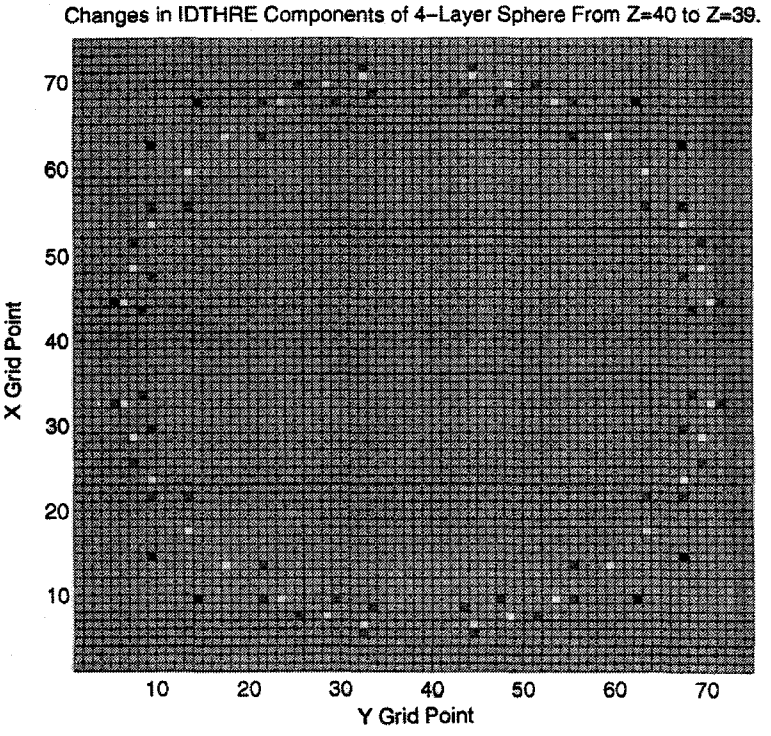

Fig. 4. The changes in the z-directed component of the material IDs from the plane $z = 39$ to $z = 40$ in the four-layer sphere. The outer black squares indicate a change from LWC bolus to the surrounding free space; the outer gray squares, skin to LWC bolus; white squares, from bone to skin; and inner gray squares, from brain to bone.

$92 \times 95 \times 92$ cell oversized mesh, in which is positioned a head model consisting of a series of concentric rings designed to simulate skin–skull–brain interfaces. This research shows that FDTD analysis of a sphere of HWC tissue varies only slightly from the analytical solution. However, a few difficulties with using FDTD for this type of problem were also brought to light. The analysis uses a total field calculation with source distribution defined point-for-point along the surface. Originally, this field was given as a surface distribution. This distribution on the "stair-step" approximation to the curved surface left several holes in the source field for which the electric field was unspecified. Large amplitude spikes resulted, along with incomplete coupling to the sphere. To remedy this problem, a volumetric source distribution is defined. This eliminates the holes in the distribution and provides complete coupling into the HWC tissue.

A second problem identified by the laminated sphere runs is "staircase spikes" produced along the material boundaries. These spikes are discretization errors caused by cubical cells approximating the curved surfaces of the spherical shells. At interfaces between dielectrics with differing conductivity and dielectric constant, the tangential electric field is continuous, while the normal electric field jumps in inverse proportion to the ratio of complex permittivity. Electric field oriented almost tangentially to one of these boundaries will exhibit a small discontinuity. However, if the boundary is approximated by cubical cells, at some isolated cube faces the electric field will appear to be entirely normally directed, and hence experience an unrealistically large discontinuity.

Figs. 3 and 4 demonstrate this staircase spike effect. Fig. 3 shows the electric field strength across a central x-y slice (where y varies left to right across the face, x varies back to front, and z increases with height from neck to the top of the head) of a four-layer laminated sphere with HWC tissue simulating the brain from the center to a radius of 32 cells (about 9.7 cm), LWC simulating the skull two cells thick, a single cell layer of HWC tissue simulating skin, and the four remaining cells exterior to the idealized spherical head within the spherical source assigned LWC parameters. Since the electric field is specified for all time on the spherical surface surrounding the head, the specification of the medium outside the source and absorbing boundary conditions are unnecessary. This geometry does not correspond to that of the three-layer analytic model described above. Instead, the exaggerated skull radius—with higher power levels—is used here to most clearly show the discretization errors. For this plot, lighter coloring corresponds to higher electric field strength. The focal target is easily seen as the white area in the center. One can also see several isolated spikes of high electric field strength near the maximum radius. These staircase artifacts are easily attributed to discretization error by comparing Fig. 3 to Fig. 4. Fig. 4 is a plot of the changes in the z-directed material parameters from the layer slice shown in Fig. 3 ($z = 39$) to the adjacent layer ($z = 40$). Wherever a pixel is highlighted, there is a small discrete horizontal edge where the edge should be continuously curving.

One additional disadvantage of using FDTD for this hyperthermia study is that the intended excitation is a 915 MHz continuous wave. A peak-field value storage array must be incorporated to allow for a simple conversion from time-domain electric field values to frequency domain time-averaged power density over the volume of interest. This also reduces the

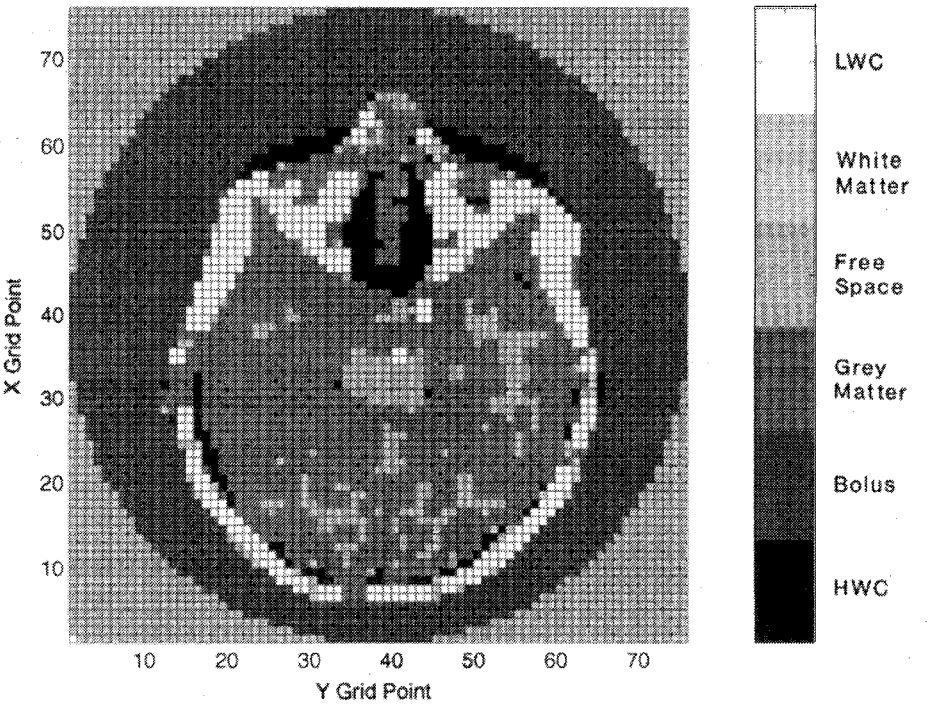

Fig. 5. Central x-y cut of the head model showing the ID values at $z = 38$.

TABLE I

Material ID #	Material Type	Relative Permittivity ϵ'	Conductivity σ (S/m)
1	HWC: Skin	51	1.3
2	Bolus	51(HWC)/6(LWC)	1.3(HWC)/0.1(LWC)
3	Grey Matter	45	1.0
4	Free Space	1	0.0
5	White Matter	37	0.7
6	LWC: Bone/Fat	6	0.1

plethora of information from FDTD analysis to a more manageable level.

Despite these drawbacks, the inherent simplicity, ease of validation, and availability of FDTD-suitable biological data dictated the use of the FDTD method. Both the general-purpose three-dimensional FDTD FORTRAN code and a finely discretized MRI-scan-based human head model developed at Pennsylvania State University were employed in this study [12]. This excellent, user-friendly code greatly contributed to the efficient implementation of the numerical analysis.

The head model is a four-tissue computer model of an actual *in vivo* human head developed from an MRI scan. Each tissue type mapped by the MRI was then assigned representative electromagnetic properties based on measured values reported by Stuchly and Stuchly [13]. For the focused heating analysis, the space between the head model and the source distribution is modeled as a liquid bolus, with either of two possible characteristics. One characteristic is associated with LWC tissue and is referred to as the "bone-like bolus." The other uses HWC tissue parameters and will be called the "muscle-bolus." A bone bolus might model a nonaqueous bolus matching medium, such as mineral oil. A cross-sectional cut of the head model is shown in Fig. 5. The corresponding electrical characteristics are given in Table I.

The original head mesh was based on a cell size of 3.22 mm, but this mesh size results in a head too large to fit within the original source radius of 9.45 cm. To fit the entire head within the source distribution, the cell size was arbitrarily reduced to 2.55 mm to study the effects of inhomogeneous media on overall heating performance. Following this study, computation was performed with the full-sized head with source scaled to the larger radius of 12 cm. As shown in the three-layer analytic model, the shell of bone and the slightly lower conductivity of gray matter compared to nonspecific HWC tissue allows a larger radius source.

IV. Results

Four computational runs are presented to show the validation of the analytically optimized spherical source distribution discussed above. Since only the tangential source electric field needs to be specified in the FDTD computation, details of the spherical harmonics throughout the tissue volume are unnecessary. From (1), it is clear that the θ-directed electric field component of each mode has constant phase at a given radius. Also, the optimization coefficients, A_1, A_3, and A_5, were

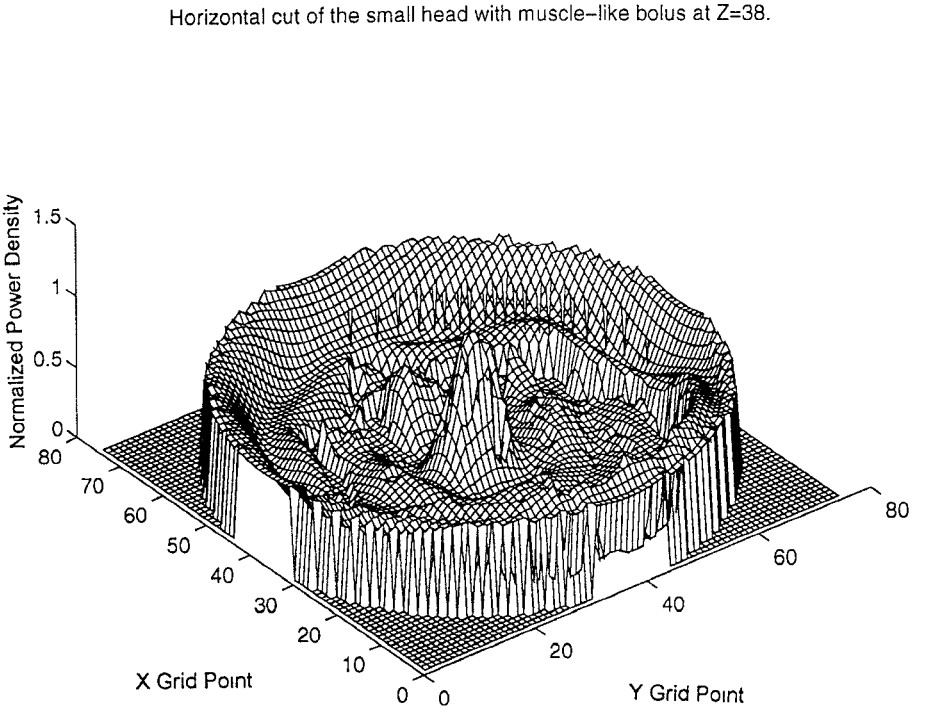

Fig. 6. Power density across the central x-y plane of the small head model with a muscle bolus, normalized to the value at the center.

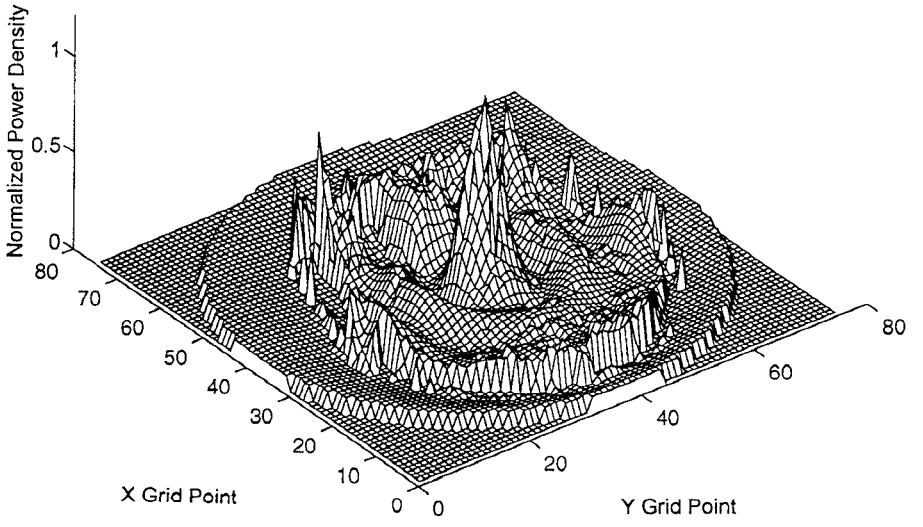

Fig. 7. Power density across the central x-y plane of the small head model with a bone bolus, normalized to the value at the center.

originally determined for maximum destructive interference at the sphere surface, which occurs when the higher-order mode maxima are 180° out of phase with the fundamental mode maximum at the surface. Thus, the surface excitation for the FDTD computation is entirely real, and its amplitude varies according to the relation [8]:

$$A(\theta) = \sin\theta + 0.2365\sin 3\theta + 0.0640\sin 5\theta. \quad (2)$$

Figs. 6–9 show 3-D plots of the power density distribution across a central x-y slice of each of the runs. These plots present power density levels in the plane passing through the center of the head running from ear to ear and through the middle of the nose, normalized (in each case) to the power density level at the center. The maximum at the center of each plot is the location of the focal target. The power density across the small head with a muscle bolus is shown in Fig. 6. This plot clearly shows a distinct focus at the center of the head. The power density at this focus reaches the same strength as

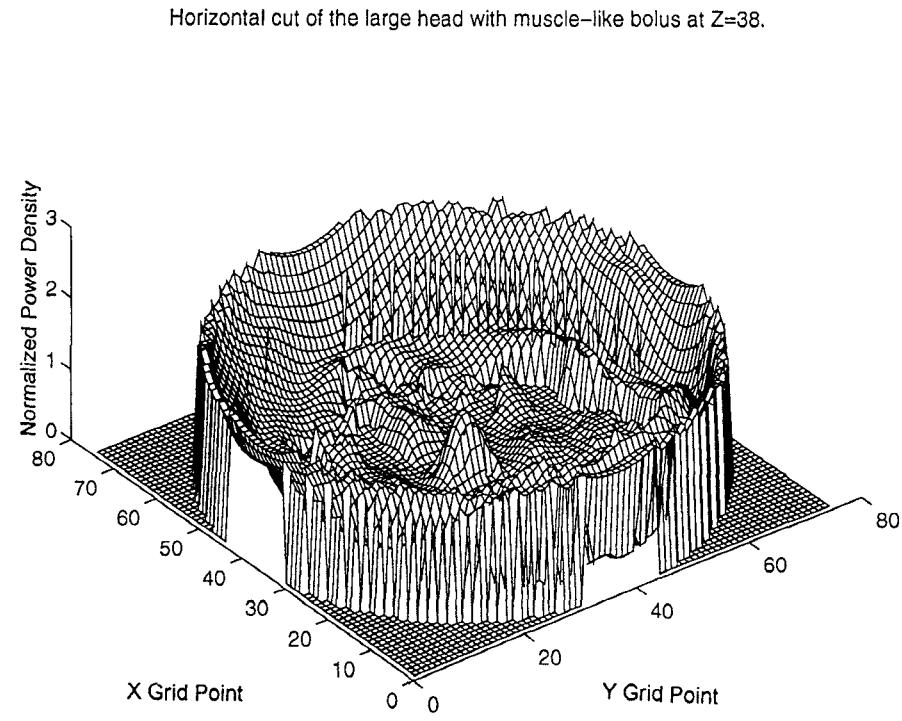

Fig. 8. Power density across the central x-y plane of the large head model with a muscle bolus, normalized to the value at the center.

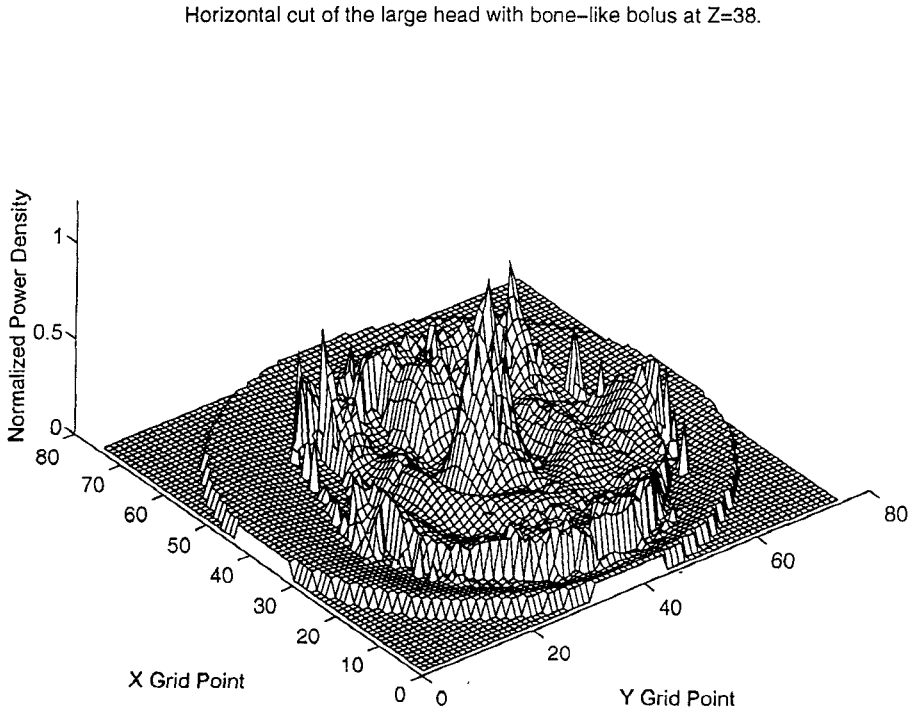

Fig. 9. Power density across the central x-y plane of the large head model with a bone bolus, normalized to the value at the center.

the power density at the very edge of the bolus. It can be seen from this plot that the power density is significantly reduced inside the skin of the actual head model. Because the bolus fluid could be circulated and cooled, the excessive heating in the bolus is irrelevant.

Fig. 7 shows the power density pattern across the small head model with a bone-like bolus, using the surface excitation given by (2). As can be seen in this plot, there is still a focus; however, the power density level in the bolus fluid is much lower than for the HWC bolus case. The edges of the head model also contain more isolated singularities than are present with the muscle bolus. In addition, the focus is seen to be less centralized. This is due to defocusing in the bone bolus, which is thick near the front and sides of the head and relatively thin near the back. This asymmetry shifts the focal position and broadens the peak.

These runs done on small head models show that the power density throughout the head is significantly less than the power density at the focus. The overheating occurs predominantly within the bolus, an area which is not of concern relative to overheating healthy tissue. This fact led to the runs on a full-sized head model with a 24-cm-diameter source. The results for these runs are shown in Figs. 8 and 9. These show results similar to those of Figs. 6 and 7; however, the bolus is subjected to much higher power levels. In both cases, there is a centered global maximum at the focal target, with no excessive power deposition in any surrounding healthy tissue. The numerically computed patterns are remarkably similar to those computed analytically, with only small-scale variations of power within the head volume generated by the tissue inhomogeneities.

The focal resolution can be measured by examining the average power density value in the nine cells around and including the center of the sphere. These values are found to be: 0.88 for the small head with muscle bolus, 0.90 for the small head with bone bolus, 0.84 for the full-sized head with muscle bolus, and 0.91 for the full-sized head with bone bolus. Since the power density level at the exact center is unity for all cases, lower center mean power density indicates a sharper focus. The full-sized head with muscle bolus has the highest spatial resolution. Another measure of the focusing performance of this spherical source is the total normalized mean power density level across the entire head volume. For a fixed power density level of unity at the central focus, a lower average power density across the volume indicates a greater concentration of power in the focal region. For the same four cases, the total mean values are: 0.11, 0.22, 0.24, and 0.29. The small head model values indicate less power outside the focal region, since there is less head tissue in the larger radius regions of the power pattern where power grows rapidly.

Other isolated spikes occur throughout the head volume, but in all cases, since they are narrower than both half the shortest tissue wavelength and the thinnest tissue layer, they can be attributed to discretization artifacts. Even without removing these artifacts, the total number of cells within the head that are exterior to the focal region with power density values above unity—at which thermal damage begins—is quite small, varying from 0.01% for the small head with muscle bolus, to 1.66% for the full-sized head with bone bolus. As these are well-distributed and greatly separated, the thermal conduction and perfusion of surrounding tissue limits the heat damage.

V. Conclusion

A numerical analysis using the FDTD method on MRI-scan-based head model demonstrates for the first time that irradiating a deep-set tumor with an idealized noninvasive microwave source is possible with proper source optimization. The results show that even with no optimization to account for the presence of actual human head inhomogeneities, reasonable focusing precision at depth is possible. These simulations have also demonstrated that a muscle-like bolus is preferable to a bone-like bolus, yielding a sharper focus, as well as less excessive heating elsewhere in the head.

Further study is needed to improve the focusing of external noninvasive sources. In particular, by varying the source distribution, the focal maximum can be arbitrarily repositioned. Combinations of these different source distributions may yield specifically tailored power patterns for tumors with particular shapes.

This research clearly indicates the need for continued research in the area of microwave hyperthermia treatment of cancer, but shows that safe and effective deep focused heating in the head is theoretically possible.

Acknowledgment

The authors would like to thank Prof. R. Luebbers and D. Steich for providing the FDTD code and the MRI-based head tissue data file, and to A. Morgenthaler for many helpful discussions.

References

[1] K. Kunz and R. Luebbers, *The Finite Difference Time Domain Method for Electromagnetics*. Ann Arbor: CRC Press, 1993.
[2] D. Sullivan, "Three-dimensional computer simulation in deep regional hyperthermia using the finite difference time-domain method," *IEEE Trans. Microwave Theory Tech.*, vol. MTT-38, pp. 204–211, Feb. 1990.
[3] J. Toftgard, S. Hornsleth, and J. Bach Andersen, "Effects on portable antennas of the presence of a person," *IEEE Trans. Antennas Propagat.*, vol. 41, pp. 739–746, June 1993.
[4] E. El-Sharawy and C. Birtcher, "Magnetic shielding of cellular phone antennas," in *URSI Symp. Dig.*, June 1995, p. 127.
[5] L. Martens, J. DeMoerloose, C. DeWagter, and D. DeZutter, "Simulations of the electromagnetic fields coupled into the head by using wireless telephones," in *Progress Electromagn. Res. Symp. Dig.*, July 1995, p. 584.
[6] M. Okoniewski and M. Stuchly, "Modeling of electromagnetic fields in the user of cellular telephones," in *Progress in Electromagn. Res. Symp. Dig.*, July 1995, p. 585.
[7] J. Mooibroek, A. DeLeeuw, J. Lagendijk, A. Zwamborn, and P. van den Berg, "Clinical approach of RF-waves in regional hyperthermia induced by the Utrecht coaxial TEM system," in *Progress Electromagn. Res. Symp. Dig.*, July 1995, p. 688.
[8] C. Rappaport and F. Morgenthaler, "Optimal source distribution for hyperthermia at the center of a sphere of muscle tissue," *IEEE Trans. Microwave Theory Tech.*, vol. MTT-35, pp. 1322–1327, Dec. 1987.
[9] C. Rappaport and J. Pereira, "Optimal microwave source distributions for heating off-center tumors in spheres of high water content tissue," *IEEE Trans. Microwave Theory Tech*, vol. 40, pp. 1979–1982, Oct. 1992.
[10] J. A. Stratton, *Electromagnetic Theory*. New York: McGraw-Hill, 1941.
[11] J. A. Shaw, C. H. Durney, and D. A. Christensen, "Computer-aided design of two-dimensional electric-type hyperthermia applicators using the finite difference time domain method," *IEEE Trans. Biomed. Eng.*, pp. 861–870, Sept. 1991.
[12] R. J. Luebbers, Penn. State Univ., FDTD Code.
[13] M. Stuchly and S. Stuchly, "Dielectric properties of biological substances—tabulated," *J. Microwave Power*, vol. 15, no. 1, pp. 19–23, Jan. 1980.

David Dunn was born in Heidelberg, Germany on December 14, 1970 and grew up in Port Huron, MI. He received the M.S. degree in electrical engineering , specializing in low observables (Stealth), from the Air Force Institute of Technology (AFIT) in December 1994 He received the B.S. degree in electrical engineering from the U.S. Air Force Academy in 1993.

This is his first published paper and stems from the work related to the completion of his Master's thesis at AFIT.

Carey M. Rappaport received the S.B. degree in mathematics, the S.B., S.M., and E.E. degrees in electrical engineering in June 1982, and the Ph.D. degree in electrical engineering in June 1987, all from the Massachusetts Institute of Technology.

He has worked as a Teaching and Research Assistant at MIT from 1981 until 1987, and, during the summers at COMSAT Labs in Clarksburg, MD, and The Aerospace Corp. in El Segundo, CA. He has been on the faculty at Northeastern University in Boston, MA since 1987. He is currently Associate Professor of Electrical and Computer Engineering. He has authored more than 75 technical papers in the areas of microwave antenna design, electromagnetic scattering computation, and bioelectromagnetics, and has received two reflector antenna patents and one biomedical device patent.

Prof. Rappaport was awarded the IEEE Antenna and Propagation Society's H.A. Wheeler Award for best applications paper of 1985. He is a member of Sigma Xi and Eta Kappa Nu professional honorary societies.

Andrew J. Terzuoli, Jr. received the Ph.D. degree from the Ohio State University (OSU) in 1982, the M.S. degree from Massachusetts Institute of Technology in 1970, and the B.S. degree from Polytechnic Institute of Brooklyn in 1969, all in electrical engineering.

He has been on the faculty of the Air Force Institute of Technology since late 1982, where he is a tenured Civilian Faculty Member. Prior to this he was a Research Associate at the ElectroScience Laboratory at OSU, and a member of the technical staff at the Bell Telephone Laboratories. His research interests include computer model based studies; application of parallel computation, VLSI technology, and RISC architecture to numerical and transform methods; remote sensing; antennas and electromagnetics, machine vision and image processing; automated object recognition; wave scattering, radar cross section and low observables (Stealth) technology. He has published numerous reports and articles in journals and conference proceedings in these and related areas.